Generation of a saw-tooth bunch at AWA

G. Ha[†]

Pohang Accelerator Laboratory, Pohang, Gyeongbuk 37673, KOREA
[†]E-mail: homehe@postech.ac.kr

J. G. Power, M. Conde, E. E. Wisniewski, W. Liu, W. Gai, K.-J. Kim and A. Zholents

Argonne National Laboratory, Argonne, IL 60439, USA

Q. Gao

Tsinghua University, Beijing 100084, China

The current profile of a charged particle bunch regulates the self-generated fields that play a critical role in several applications: wakefield acceleration, radiation generation, and control over the bunch's quality. The recently developed exchange-based method of temporal manipulation provides direct control over the longitudinal phase space via transverse manipulation followed by a transverse-to-longitudinal exchange. This new method is capable of generating higher quality temporal distributions compared with previous coupling-based methods. In this paper, we introduce the principle of the exchange-based temporal shaping method, experimental demonstrations of temporal distributions generated, and describe application experiments planned at the Argonne Wakefield Accelerator facility.

Keywords: Emittance exchange, shaping, transformer ratio, Double EEX.

1.   Introduction

When a charged particle interacts with its surrounding environment, it generates various type of electromagnetic self-fields known as wakefields, synchrotron radiation, etc. Since the total radiation of a particle bunch is just the superposition of fields from the individual particles, the total radiation can be controlled by tailoring the current profile of the particles within the bunch. The ability to control the radiation benefits several applications such as: wakefield acceleration, THz/X-ray generation, and control over the bunch's quality. In light of this situation, methods to control the current profile have become an active area of research.

The saw-tooth current profile is a representative example of radiation manipulation via current profile shaping of the bunch due to its usefulness in the wakefield acceleration. This profile flattens the wakefield inside the drive bunch so that the drive bunch more effectively transfers its energy to the main bunch [1]. For completeness, we give references for several other examples of the current profile shaping for THz/X-ray generation, bunch quality control etc [2-5].

Existing shaping methods to control the current profile of the bunch include: (1) laser shaping methods which shape the temporal profile of the laser impingent on a photocathode in an RF gun [6] and (ii) coupling-methods that introduce a coupling between the *z*-

coordinate and another coordinate (x, y or δ) [7-9]. The ability of the laser shaping methods to produce high-quality profiles is limited by the difficulty of shaping the laser profile itself and space-charge effect near the cathode. The Coupling method has more applications than the laser shaping since all transverse or energy manipulation techniques can be used to control the current profile via coupling. However, this method has an intrinsic limitation since the coupling method assumes a linear relation between z and coupled coordinate. In summary, existing shaping methods are limited in their ability to produce sharp current profiles and in their capability to produce a wide variety of shapes (i.e. arbitrary shapes).

We introduce a new method to overcome the limitations of the existing shaping methods described above. The emittance exchange (EEX) beamline exchanges the transverse and longitudinal bunch properties [10]. Since the transverse properties of the bunch (including its profile) upstream of the EEX beamline are converted to longitudinal properties downstream of the EEX beamline, we can use any transverse manipulation technique to control the longitudinal properties [11]. More importantly, this method does not rely on coupling to other bunch coordinates so it avoids the intrinsic quality limitation of the coupling-based methods described above.

In this proceeding, we present the theoretical background and several experimental demonstrations of the exchange-based method. Section 2 covers the principle of exchange-based manipulation and its limiting effects. Section 3 shows the experimental set-up and demonstrations. In section 4, we introduce several planned experiments and their preliminary simulation results.

Note, all content in this proceeding was previously published in Ref [12-18].

2. Exchange based shaping

EEX was first proposed in Ref [19] using a chicane with a deflecting cavity in between two doglegs. This beamline provided an incomplete EEX due to the residual coupling between the transverse and longitudinal phase space. This incompleteness was resolved a few years later by adjusting the beamline from a chicane to a double dogleg [10]. This proceeding is based on the double dogleg type EEX beamline.

The bunch dynamics through the EEX beamline are described by a 4D transfer matrix. In this matrix, diagonal matrices describe transverse-to-transverse and longitudinal-to-longitudinal contributions while off-diagonal matrices show transverse-to-longitudinal and longitudinal-to-transverse couplings. Since the EEX beamline provides complete exchange of transverse and longitudinal phase space, the transfer matrix of EEX beamline with rectangular dipole magnets is expressed as [10],

$$\begin{pmatrix} x_f \\ x_f' \\ z_f \\ \delta_f \end{pmatrix} = \begin{pmatrix} 0 & 0 & \kappa(L+L_D) & \eta+\kappa\xi(L+L_D) \\ 0 & 0 & \kappa & \kappa\xi \\ \kappa\xi & \eta+\kappa\xi(L+L_D) & 0 & 0 \\ \kappa & \kappa\xi & 0 & 0 \end{pmatrix} \begin{pmatrix} x_i \\ x_i' \\ z_i \\ \delta_i \end{pmatrix}, \qquad (1)$$
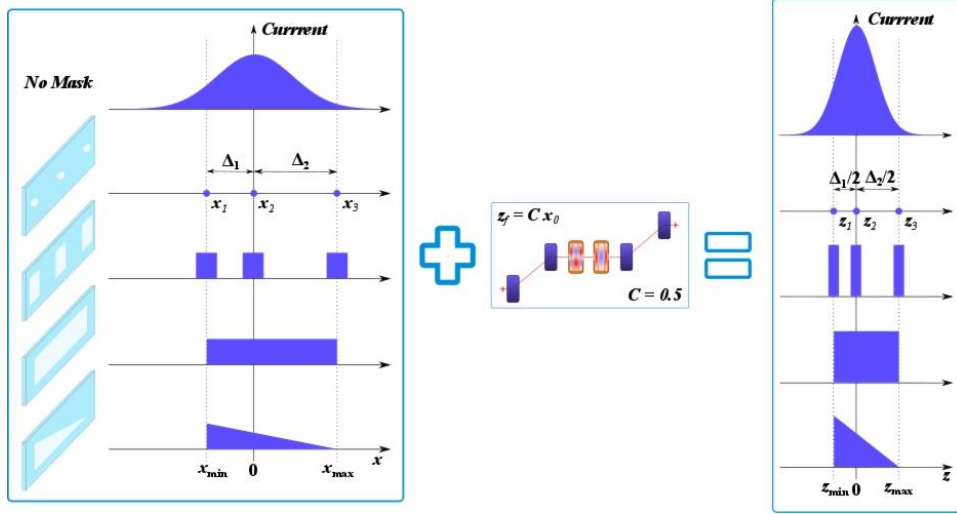
Fig. 1. Conceptual drawing of transverse-to-longitudinal profile conversion (figure from Ref. [12]). Linear scaling factor is assumed to 0.5. EEX beamline has both deflecting cavity (first) and fundamental mode cavity (second) to eliminate thick-cavity effect.

where κ is the kick strength of the deflecting cavity, L, η, and ξ are the effective length, dispersion and momentum compaction factor of the dogleg, and L_D is the drift length between the dogleg and the cavity. When $1 + \kappa\eta = 0$ holds, the double dogleg EEX beamline provides the matrix of Eq. 1 which has the unique feature of zero diagonal terms and non-zero off-diagonal terms. $1 + \kappa\eta = 0$ is called the EEX condition and the matrix shows that the final longitudinal characteristics are determined by the initial transverse terms and vice versa.

According to Eq. 1, the final longitudinal position of the particle (z_f) is determined by its initial transverse position (x_i) and momentum (x_i'). Since x_i and x_i' have a linear relation ($S_x = x_i'/x_i$) in linear theory, we can re-write z_f as function of x_i [12].

$$z_f = C_0 x_i, \tag{2}$$

where $C_0 = \kappa\xi + S_x\{\eta + \kappa\xi(L + L_D)\}$. Since z_f is a linearly proportional to x_i, the final current profile scales with the initial transverse profile. In this way, we can generate arbitrary current profiles by manipulating the transverse profile as shown in Fig. 1.

2.1. *Nonlinear effects and collective effects in EEX-shaping*

Exchange-based shaping is ideal in linear theory (emittance effect and thick-cavity effect can be eliminated using quadrupoles [20] and fundamental mode cavity [21]) as shown in Eq. 2. However, nonlinear effects and collective effects introduce additional terms to Eq. 2 as [12],

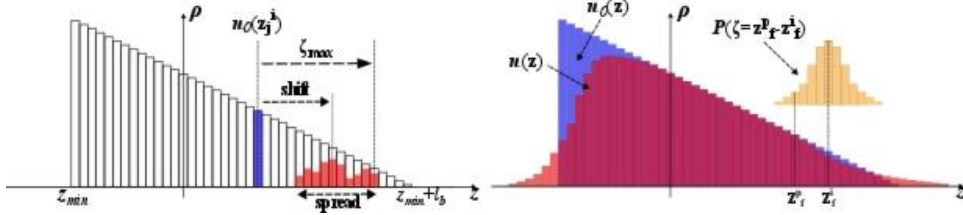$$z_f = C_0 x_i + T_{5nm}X_n X_m + \xi\Delta\delta, \tag{3}$$

Fig. 2. Conceptual figure to show how the nonlinear and collective effects perturb the ideal profile (left) to create the actual profile (right). This figure was taken from Ref. [12].

where T_{5nm} is the second order coefficient of the EEX beamline (third or higher is ignored since their contribution to the bunch length is less than 5%), $X = \{x, x', y, y', z, \delta\}$, and $\Delta\delta$ is the integrated energy change due to the space-charge effect and coherent synchrotron radiation (CSR). These extra terms perturb the particle location from its ideal final position (Eq. 2) to a shifted position (Eq. 3). For a bunch profile, its final distribution is shifted about the ideal position as shown in Fig. 2. These perturbations result in perturbation of the ideal shaped profile.

The second order effects have thirteen non-zero terms,

$$\zeta_{2nd} = C_1 x_i^2 + C_2 x_i x_i' + C_3 x_i'^2 + C_4 z_i^2 + C_5 z_i \delta_i + C_6 \delta_i^2 + C_7 x_i z_i + C_8 x_i' z_i$$
$$+ C_9 x_i \delta_i + C_{10} x_i' \delta_i + C_{11} y_i^2 + C_{12} y_i y_i' + C_{13} y_i'^2, \tag{4}$$

where ζ_{2nd} is the deviation due to the second order terms, and C_i are the second order coefficients (coefficients are described in Ref. [12]). Based on Eq. 4, we can find a simple method to suppress the second order effects and we call this the *slope-control method*. If we consider the x-terms in Eq. 4, we observe that x_i and x_i' have a linear relationship, and therefore the mean shift and spread of the particles can be written as [12],

$$\langle\zeta\rangle = (C_1 + C_2 S_x + C_3 S_x^2)\langle x_0^2\rangle, \tag{5}$$

$$\langle\zeta^2\rangle = (C_1^2 + 2C_1 C_2 S_x + (2C_1 C_3 + C_2^2)S_x^2 + 2C_2 C_3 S_x^3 + C_3^2 S_x^4)\langle x_0^2\rangle. \tag{6}$$

Both the mean shift and spread have to be minimized to suppress the perturbation of the profile. Since both of them have the slope related terms as a coefficient, we can find appropriate initial horizontal slope to minimize these terms. All other terms follow the same logic.

We begin by examining the second order effects on the shaped profile. Figure 3 shows the shaped current profiles after the EEX beamline and the corresponding deviation of the transformer ratio. (Note that in the figure the ideal profile is triangular and the deviation of transformer ratio is divided by ideal transformer ratio. i.e. $(R - R_0)/R_0$.) The simulation is performed using GPT without collective effects in order to characterize the second order effects. In the figure, we change the horizontal, longitudinal and vertical slopes one at a time (while keeping the others fixed) over a range that includes the "suppressing value". Colors in (a-b), (c-d), and (e-f) correspond to the incoming horizontal, longitudinal, and vertical slopes, respectively. Each incoming slope clearly controls the final current profile, and the deviation of transformer ratio is minimized at the suppressing value of the slope which agree well with the theoretically estimated values [12]. Incoming slopes can be
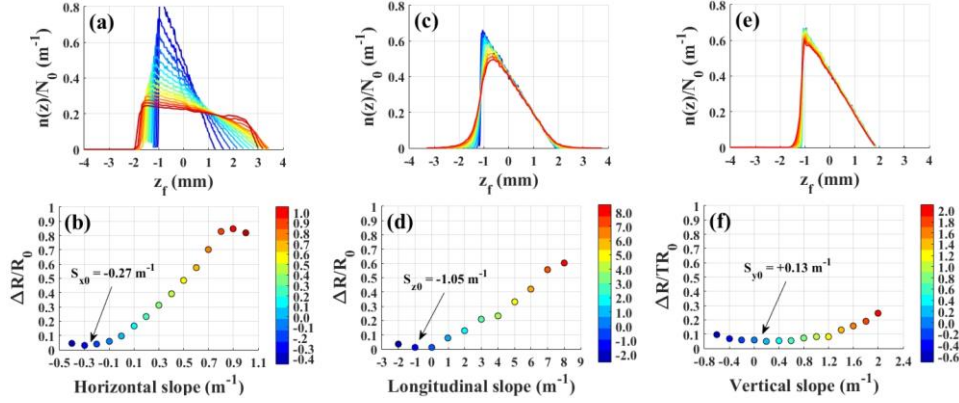
Fig. 3. Shaped final current profile with different incoming (a) horizontal, (c) longitudinal, and (e) vertical slopes. Deviations of transformer ratio from its ideal value correspond to (b) horizontal, (d) longitudinal, and (f) vertical slopes. These are simulated results without collective effects. (figure from Ref. [12])

easily controlled using the quadrupole magnets for the transverse and the linac phase for the longitudinal. The experimental demonstration of this method will be discussed in Section 4.

Next we examine the collective effects on the shaped profile and treat the collective effects as integrated single kicks from each major beamline element (dogleg and deflecting cavity). Once it is written as a single term, their evolution along the EEX beamline can be tracked and it appears in Eq. 3 as [12],

$$\zeta_{col} = \xi_2(1 + \kappa\eta^*)\Delta\delta_1 + \xi_2\Delta\delta_2 + \xi_2^*\Delta\delta_3, \tag{7}$$

where ξ_2 is the momentum compaction factor of the second dogleg, and $\Delta\delta_i$ are the integrated momentum change through the first dogleg ($i = 1$), drift and the cavity ($i = 2$), and the second dogleg ($i = 3$). Notice that all three collective effect terms have ξ_2 as a coefficient so decreasing ξ_2 would suppress the total collective effect on the shaped profile. This can be done by decreasing the bending angle of the second dogleg while increasing the drift length of the second dogleg in order to preserve the dispersion (η) need to
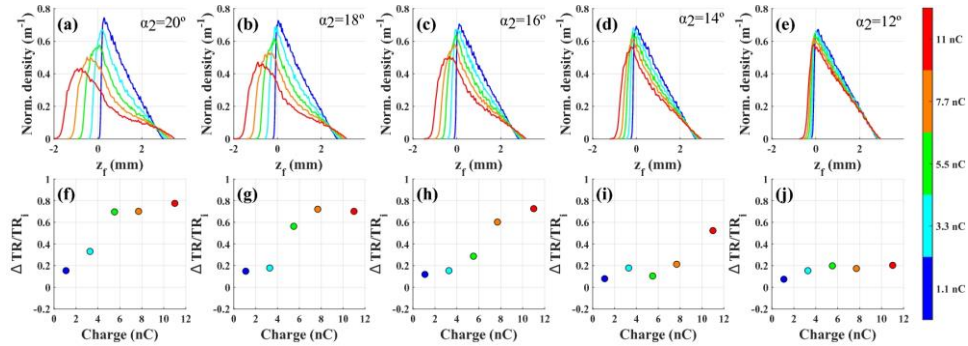

Fig. 4. Shaped current profiles and corresponding deviation of transformer ratio. All physics is included and the bunch energy is 50 MeV. Colors correspond to the total charge of the bunch. Bending angle of the second dogleg decrease by 2° from the 20° for the first column. (figure from Ref. [12])

maintain the EEX condition. We call this the asymmetric dogleg method to suppress the collective effects.

The GPT simulation results shown in Fig. 4 support the feasibility of this asymmetric dogleg method. When a 12° bending angle (e) is used for the second dogleg instead of 20° (a), it reduces ξ_2 from 0.29 m to 0.18 m. In terms of the deviation of the transformer ratio, the 12° case stays around 0.2 even when the total charge is 11 nC. Compare this to the 20° case, where a 3.3 nC charge has deviations greater than 0.3. This difference is clear in the profiles too.

2.2.   *Emittance growth from CSR*

In addition to the nonlinear and collective effects on the shaped profile, emittance preservation is another important issue to realize in exchange-based temporal shaping. Many methods have been developed to minimize emittance growth in well-known dispersive beamlines (e.g. chicane) since they have been in use for many years. In these beamlines, the collective effects only directly change the longitudinal phase space and it is the dispersion of the beamline that introduces these effects into the transverse phase space. As a result, the collective effects increase the projected transverse emittance but does not change the slice emittance. In contrast, for the EEX beamline, the collective effects directly change both the transverse and longitudinal phase spaces due to the exchange of phase spaces. As a result, the collective effects increase both the projected and slice transverse emittance in the EEX beamline. Emittance growth becomes even more serious in the double EEX beamline which uses two double dogleg EEX beamlines in series.

We first study emittance increase in an EEX beamline for a high charge case. Fig. 5 shows the horizontal emittance after a double EEX beamline [13]. The initial horizontal emittance is 10 μm, and the charge and energy of the bunch are 5 nC and 50 MeV. Using GPT, we turn on space charge and nonlinear effects but turn CSR off and the final emittance increases to ~30 μm. This is a large growth but acceptable for a high charge bunch. However, when CSR is turned on the emittance increases from 30 μm to 330 μm as shown in index 1 of Fig. 5 which shows that CSR is the dominant source of emittance growth at this energy and charge.

As described above, CSR in an EEX beamline increases both slice and projected emittance. The asymmetric dogleg method can suppress the projected emittance growth (330 μm to 270 μm), but it is not enough since it does not handle the slice emittance growth. Due to the slice emittance growth, our numerical investigation has shown that the most effective method for suppressing the CSR effect is to use CSR shielding [22]. The shielding option in the GPT CSR module from Ref. [23] is applied to the simulation. When a gap size of 5 cm is applied, the emittance decreases from 330 μm to 180 μm and it goes down to 70 μm with 2 cm gap.

To suppress the emittance growth even further, the bunch has to be matched to the beamline and the CSR in the beamline. When CSR induces an emittance growth, the emittance growth can be formulated as [14],
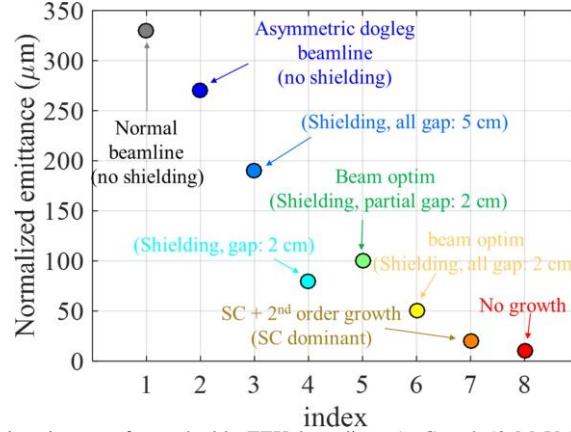
Fig. 5. The horizontal emittance after a double EEX beamline. 5 nC and 50 MeV bunch is used for GPT simulation. Initial horizontal emittance is 10 μm. (figure from Ref. [13])

$$\Delta\varepsilon = \langle x_i^2 \rangle [\{\kappa L \Delta_z - A\Delta_\delta\} S_x + \kappa(\Delta_z - \xi\Delta_\delta)]^2 + \frac{\varepsilon_{x,i}^2}{\langle x_i^2 \rangle} \{\kappa L \Delta_z - A\Delta_\delta\}^2, \tag{8}$$

where $A \equiv (\eta + \kappa\xi L)$. Note, the thick-cavity terms are ignored and the integrated kick concept in Section 2 is used in this equation too. Since CSR terms are entangled with bunch and beamline parameters, these parameters have to be optimized to minimize the emittance growth. We set a reasonable bunch size and slope to minimize the emittance growth, and we applied a gap size of 2 cm for the dipole magnet chambers and a gap size of 5 cm to the rest of the beamline for the easy bunch transport. Index 5 in Fig. 5 corresponds to this case, and the final emittance is 100 μm (compared to 180 μm without optimization). If the gap size is 2 cm along the whole beamline it decreases to 50 μm (compared to 70 μm without optimization) which is tolerable.

For the case of low charge, CSR shielding and optimization shows excellent results. Fig. 6 (b) and (c) shows the ratio of final to initial emittances of a single EEX beamline. A shielding gap of 2 cm is applied for both cases, and the bending angle of the dogleg is 20 degree for (b) and 5 degree for (c). The initial emittance was 1 μm for 100 pC and 50 MeV bunch, and it increases to 1.15 μm for (b) and 1.1 μm for (c).
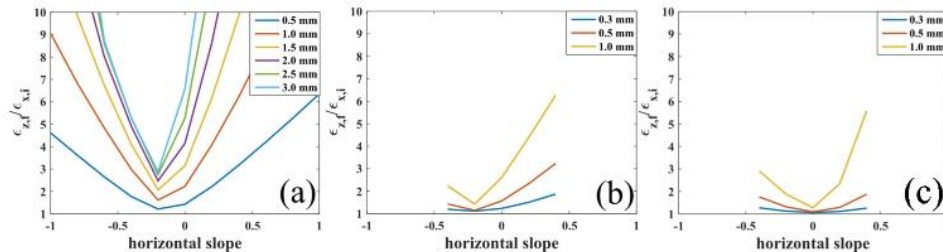
3. Experimental demonstration

Fig. 6. Ratio of final to initial emittances in single EEX beamline (figure from Ref. [14]). The bending angle of doglegs are 20 degree for (a) and (b) while (c) uses 5 degrees. CSR shielding is not applied to (a) for the comparison and (b) and (c) use 2 cm gap shielding for the whole beamline.
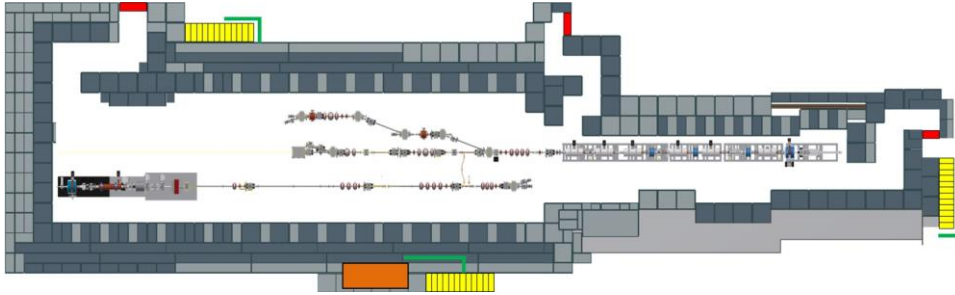
Fig. 7. Configuration of Argonne Wakefield Accelerator facility.

Exchange-based temporal profile shaping was experimentally demonstrated in 2016 [15], and its application to achieve a high transformer ratio in a collinear wakefield accelerator was demonstrated in 2017 [18]. These experiments were performed using a double dogleg EEX beamline installed at the Argonne Wakefield Accelerator (AWA) facility. This section briefly introduce the AWA facility and the experimental results.

3.1. *Argonne Wakefield Accelerator*

The Argonne Wakefield Accelerator facility is accelerator R&D facility at Argonne National Laboratory [24]. The AWA program develops structure-based wakefield acceleration and other bunch dynamics topics for the future colliders. Recently, this facility is changed to an accelerator R&D user facility and trying to contribute on various accelerator research area.

The facility has two rf photoinjector linacs and a cathode test stand (Fig. 7, the cathode test stand not shown). The beamline on the bottom is called the witness beamline which consists of a L-band rf photocathode gun (Mg cathode) with a single L-band accelerating cavity. This beamline generates 0.1-10 nC bunch and accelerates the bunch up to 15 MeV. Downstream of this beamline is a flexible experimental area that can be easily re-configured for each experiment. The other beamline is called the drive beamline which consists of a L-band rf photocathode gun (Cs_2Te cathode) with six L-band accelerating cavities. The high QE cathode in this beamline generates 0.1-100 nC for single bunch, and it can generates up to 32 bunches using an optical laser split/delay stage. Downstream of this beamline is also a flexible experimental area. The EEX beamline is installed at the downstream of the drive beamline. The cathode test stand has an rf gun with a variety of diagnostics to study cathode development and field emission.

The AWA facility has several unique features which strongly benefits user experiments. First, this is the only facility that generates a high charge bunch (10-100nC). This is an important feature for most of the beam-driven wakefield accelerator schemes. Second, experiments using two bunches can be done at this facility by: (1) applying two temporally separated laser pulses in the same rf gun, as is done in other facilities, (2) using the independent drive and witness beamlines which provides independent timing and bunch quality control, and (3) the EEX beamline provides controllability on the longitudinal phase space. More details on the facility can be found in Ref. [24].

3.2. *Property exchange and temporal profile shaping*

A double dogleg EEX beamline was installed at the Argonne Wakefield Accelerator (AWA) facility. The bending angle of the dogleg is 20° and the separation between the dipoles is 2 m. These parameters provides a dispersion of 0.89 m and momentum compaction of 0.3 m. A 3-cell (half-full-half cell) transverse deflecting cavity is located between the two doglegs, and is operated at an rf power level of 1.0-1.3 MW to meet the EEX condition. Four quadrupoles and masks are located upstream of the EEX beamline to manipulate the transverse bunch properties (size and slope) and the horizontal profile. The drive linac phase was adjusted to control the longitudinal chirp. The nominal operating conditions of the bunch are 50 MeV and 1-10 nC and the transmission through the mask is 20-40%.

The first demonstration performed was of property exchange in the EEX beamline. One of the four upstream quadrupoles is varied while the transverse and longitudinal bunch images are monitored downstream of the EEX beamline using YAG screens and a deflecting cavity. Fig. 8 shows the bunch images with three different quadrupole settings [13]. (a), (b) and (c) corresponding to the quadrupole gradient of -0.7, 0.0, and +0.7 T/m. The horizontal bunch sizes are measured as 10.5 mm, 9.1 mm and 10.2 mm, respectively, while the vertical bunch size is fully focused or defocused depending on the quadrupole gradient. This means that the incoming horizontal properties does not affect the final horizontal properties. On the other hand, the measured longitudinal bunch lengths are 4.9 mm, 3.2 mm and 1.4 mm for the quadrupole gradients of -0.5, 0.0, and +0.5 T/m, respectively. These result clearly show that the bunch is longitudinally focused or defocused instead of horizontal focusing or defocusing when it passes through the EEX beamline. This is a clear demonstration of property exchange required by the zero-diagonal feature of the transfer matrix.
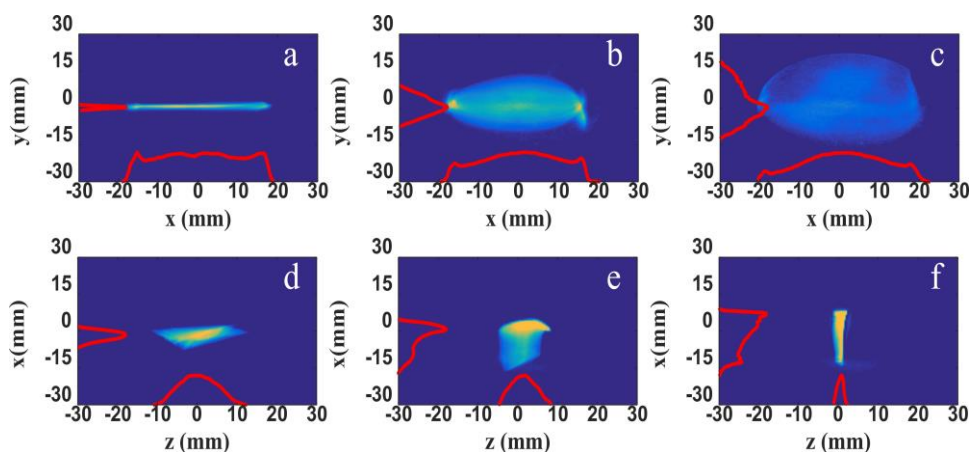

Fig. 8. Electron bunch images after the EEX beamline with different quadrupole gradients. This quadrupole is located in front of the EEX beamline to control incoming transverse bunch condition. The top row shows the transverse image of the bunch with the quadrupole gradient of (a) -0.7 T/m, (b) 0 T/m, and (c) +0.7 T/m. The bottom row shows the x-z images of the bunch using a deflecting cavity providing vertical time-dependent kick with the quadrupole gradient of (d) -0.5 T/m, (e) 0 T/m, and (f) +0.5 T/m.
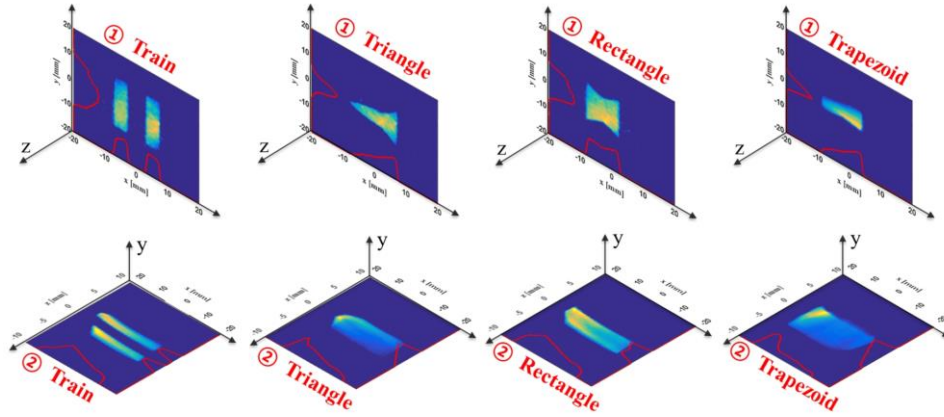
Fig. 9. Transverse bunch images are taken before the EEX beamline (top) and x-z images are taken after the EEX beamline using a deflecting cavity (bottom). Tungsten masks with different shapes are applied to the bunch before the EEX beamline to shape the horizontal profile of the bunch to train, triangle, rectangle and trapezoid.

Four tungsten masks with different shapes were used to demonstrate arbitrary current profile generation. The masks were used to shape the initial (before the EEX beamline) transverse profile of a 5 nC and 50 MeV bunch (Fig. 9, top row shows x-y images) into: a train, a triangle, a rectangle and a trapezoid. The final current profiles (after the EEX beamline) are measured using the deflecting cavity kicking the bunch vertically. The bottom row of Fig. 9 shows x-z images of the bunch after the measurement deflecting cavity [15]. Notice that these final horizontal profiles (bottom row) have lost their initial horizontal profiles (top row) and have a similar pattern; x>0 is bright and x<0 is faint. On the other hand, the final current profiles have taken on the shape of the initial horizontal profile and have become: train, triangle, rectangle, and trapezoid. This result demonstrates the feasibility of arbitrary current profile generation.

As discussed in section 2, the nonlinear effects and collective effects degrade the shaping quality. The slope-control method (described above) is experimentally demonstrated using the four quadrupoles and the linac phase. The blue curves in Fig. 10 show the initial horizontal profiles and the red curves show the final current profiles [15]. The horizontal, vertical and longitudinal slopes are initially optimized to minimize the second order effects. The blue and red curve shows reasonable agreement. When the horizontal slope is set to other values, the final current profile has a convex feature on the ramp. This result shows a good agreement with theory and simulation given in Ref. [12]. Vertical slope and longitudinal slope are also varied from their theoretical values and they also show their own unique aberration which agrees well with theory and simulations.
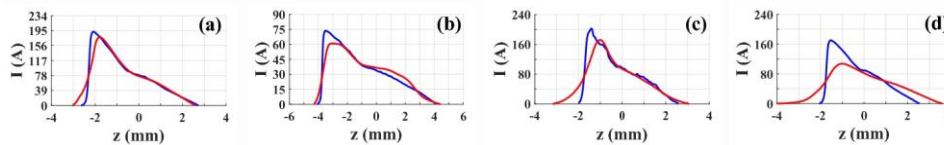

Fig. 10. Initial horizontal profile (blue) and final current profile (red) with different incoming slopes. (a) x, y, and z slopes are set to suppression values. (b) x-slope is off from the suppression condition. (c) y-slope is off from the condition. (d) z-slope is off from the condition.

3.3. *High transformer ratio from temporal shaping*

Building on the successful demonstration of temporal shaping an experiment to achieve high transformer ratio was performed. This application is a key component of a working collinear wakefield accelerator. A dielectric lined structure (DLS) is installed at the downstream of the EEX beamline to observe the enhanced transformer ratio (see Fig. 11) [18]. 150 μm thick quartz layer ($\epsilon_r = 3.75$) is sitting on the copper and the dimension of the structure is a = 1.27 cm, L = 15 cm, and b is tunable from 0 to 3.1 cm. During the experiment the gap was set to 2.5 and 2.1 mm with corresponding fundamental mode frequencies of 122 and 131 GHz to confirm the predicted increase of transformer ratio by the ratio of bunch length to the wavelength [25].

The interaction of the bunch and wakefield is measured using longitudinal phase space measurement method using a spectrometer and a deflecting cavity. The wakefield inside and behind of the drive bunch can be reconstructed by comparing the longitudinal phase space with and without DLS. The reconstructed wakefield and the estimated wakefield are plotted in Fig. 11. Both of them show reasonable agreement and the measured and estimated transformer ratio are 4.94±1.24 and 4.86 respectively. This value is the highest transformer ratio achieved so far. More details can be found in [18].

4. Upgrade to double emittance exchange

An upgrade to a double EEX beamline is underway (see Fig. 12) at the Argonne Wakefield Accelerator (AWA) facility. Since a single EEX beamline exchanges the transverse and longitudinal emittance, the final transverse emittance is relatively large due to the initially large longitudinal emittance that is typical of rf photoinjectors. Therefore, adding a second EEX beamline will achieve a low final transverse emittance. In the double EEX beamline, the middle section is where the transverse phase space is manipulated to control the final longitudinal phase space.
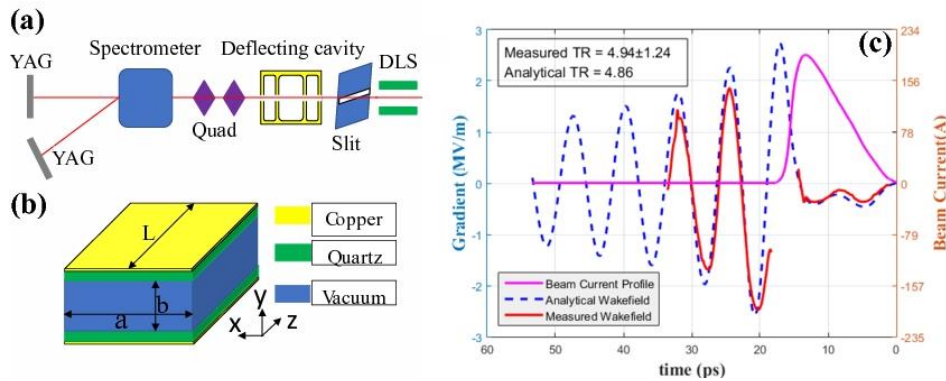

Fig. 11. (a) Layout of the downstream of the EEX beamline to measure the transformer ratio. (b) Schematic of dielectric lined structure (DLS). (c) Measured current profile and wakefield (solid) with analytically calculated wakefield using measured current profile (dashed). (figure from Ref. [18])

Fig. 12 Layout of double EEX beamline (under construction) at Argonne Wakefield Accelerator facility.

Several proof-of-principle experiments are being prepared at the AWA facility. The rest of this section introduces the idea and preliminary simulation results.

4.1. *Temporal shaping for collinear wakefield accelerators*

While the single EEX beamline already demonstrated transformer ratio enhancement via the temporal profile shaping, (1) the measured value was only ~50% of ideal value for a given bunch length and structure frequency, and (2) the relation between transformer ratio, gradient, bunch length to frequency, and profile was not thoroughly explored [26, 27]. We plan to use double EEX to (1) optimize the current profile to generate a transformer ratio greater than 10, which is higher than 80% of ideal value at the same time; and (2) to experimentally explore the relationships listed above.

Preliminary S2E simulation results in Fig. 13 show the differences between the longitudinal phase space after DLS for two different current profiles: (a) triangular and (b) door-step. Notice that the decelerating wakefield is flattened inside the bunch when the current profile is optimized (b). Also, this optimized result would provide a transformer ratio of 10 whose ideal value of the door-step is 12. The current profile can be easily controlled using the EEX beamline, and it can be measured using the deflecting cavity. The transformer ratio, gradient and the frequency of the structure can be measured using the longitudinal phase space measurement method [28].
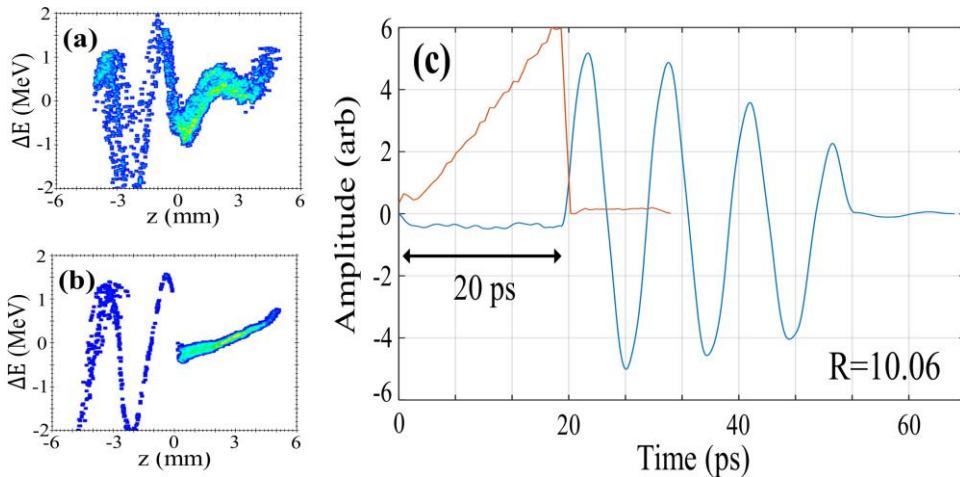
4.2. *Multi-function bunch compressor*

Fig. 13. (a) Longitudinal phase space of the bunch having triangular current profile. (b) Longitudinal phase space of the bunch having optimized current profile to maximize the transformer ratio. These simulated phase spaces are taken after the dielectric structure. The optimum current profile and corresponding wakefield is given in (c). (figure from [13])

As we can see from Fig. 8, the single EEX beamline compresses the bunch duration by focusing the bunch horizontally using quadrupoles [17]. Compared to the chicane compressor, a double EEX compressor provides three potential benefits; (1) a tunable compression ratio without an incoming longitudinal chirp, (2) a relatively easy to control current profile, and (3) a tunable final longitudinal chirp.

(1) *Tunable compression ratio.* While the chicane requires a longitudinal chirp to generate a path length difference for the compression, the EEX compressor only requires a focusing quadrupole and this compression does not require any initial chirp since the compression happens due to the exchange. Fig. 14 shows the final bunch lengths corresponding to the quadrupole settings. Q3 is the quadrupole located at the middle of double EEX beamline, and the initial bunch length can be lengthened from 0.8 mm to a final bunch of 1.0 mm or can be compressed to 0.03 mm. This is comparable to the bunch length after the second bunch compressor in LCLS.

(2) *Easy to control current profile.* A double horn profile is known to appear in the longitudinal phase space [29] after a strong compression in the chicane when the linearity in the phase space is small so that the remaining nonlinearity in the phase space becomes dominant. Although controlling the nonlinearity in the longitudinal phase space is difficult, the nonlinearity in the transverse phase space can be easily cured with nonlinear magnets (e.g. sextupole, octupole etc). Therefore, the EEX compressor potentially provides a better profile after a strong compression.

(3) *Tunable final longitudinal chirp*. The quadrupoles in the middle area of the double EEX beamline can be used to control the final longitudinal chirp as opposed to the chicane compressor that cannot control the longitudinal chirp since it is a passive beamline. S2E simulation results are given in Fig. 14. The chirp control would eliminate the necessity of dechirper or off-crest operation for the linac. Also, it can be used for the large bandwidth FEL which requires a large longitudinal chirp.
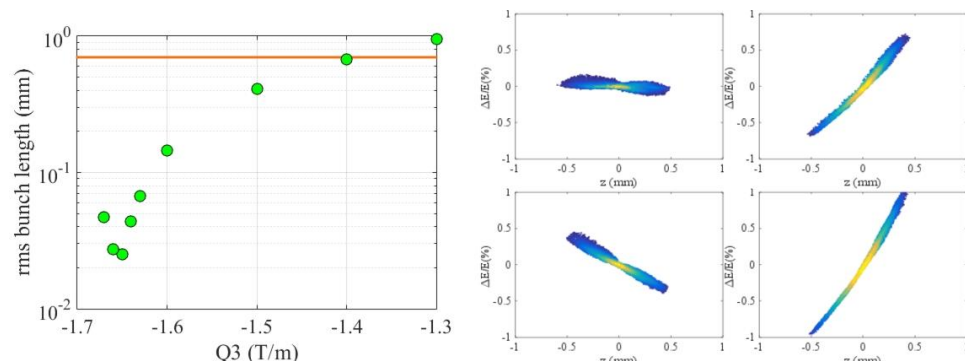
4.3. *Frequency up/down shift*

Fig. 14. Left figure shows the bunch length after double EEX compressor (green dot) and initial bunch length (orange line). Q3 is the quadrupole which is located at the middle of the double EEX beamline. Right figures show longitudinal phase spaces with different quadrupole settings which is located in the middle of the double EEX beamline. (figure from [17])
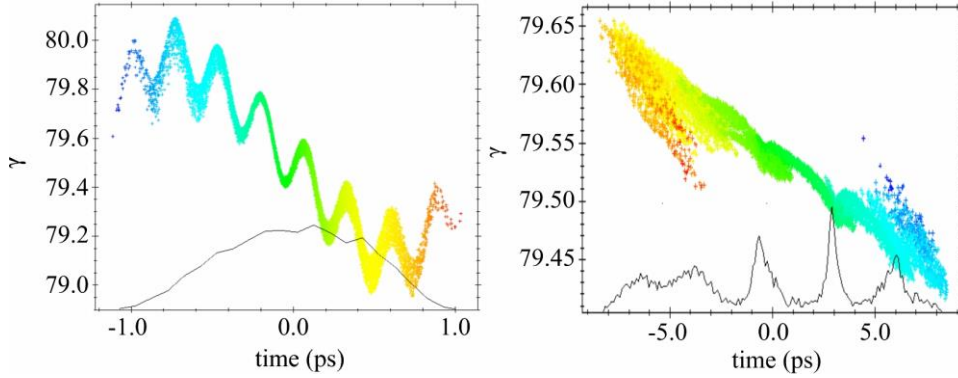
Fig. 15. Left figure shows initially energy modulated longitudinal phase space and its density profile. Right figure shows the longitudinal phase space after the double EEX beamline and corresponding density profile. The energy modulation frequency 3.74 THz, and the density modulation frequency is about 0.3 THz.

The double EEX beamline has a non-zero R56 term just like the chicane compressor. This means that the EEX beamline converts the energy modulation from a laser/undulator, wakefield structure, etc. into a longitudinal density modulation. There are several schemes to shift this density modulation to a higher or lower frequency using a bunch compression or lengthening with an energy-to-density modulation conversion. This is called frequency up/down shift, and it is normally done with a chicane.

Similar to the bunch compression/lengthening introduced in the previous section, the double EEX beamline provides more flexible bunch compression or lengthening without any requirements on the incoming longitudinal chirp. It also provides control of the final chirp. As shown in Fig. 15, any energy modulation (left) in front of the EEX beamline can be converted to the density modulation (right), and the modulation frequency can be easily controlled using the quadrupoles in the middle of the double EEX beamline.

4.4. *Transverse momentum to longitudinal density conversion*

Energy-to-density modulation conversion is a well-known method for generating high frequency modulation. In the presence of the exchange concept, we can consider another kind of modulation conversion [30]. When the bunch enters into a transverse alternating magnet array as shown in Fig. 16 (a), it will modulate the horizontal momentum as is shown in Fig. 16 (b). Since a single EEX beamline provides the exchange of transverse and longitudinal, we can convert this horizontal momentum modulation to the longitudinal density modulation as shown Fig. 16 (c).

Here the total length of the train (i.e. spacing of microbunches) depends on the initial horizontal bunch size and the slope just as bunch compression does. At the same time, the modulation strength (i.e. the gap size of alternating magnet array) determines the microbunch length. Thus, this method would control both the bunching factor and the
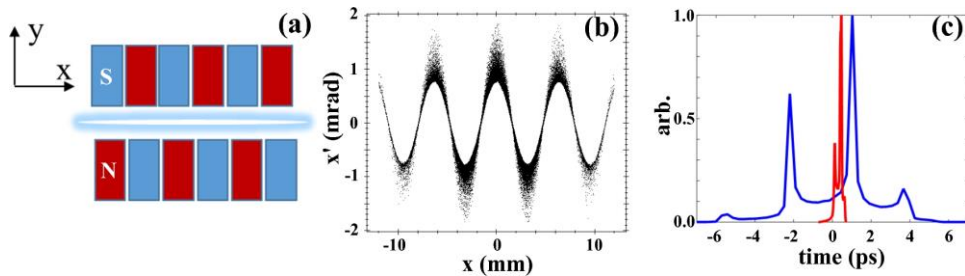
Fig. 16. (a) Transverse Halbach magnet array to generate transverse momentum modulation. (b) Horizontal phase space after the magnet array. (c) Longitudinal current profiles after the EEX beamline with different incoming bunch slope for train length control. (figure from [30])

modulation frequency with just 1-2 quadrupole magnets and the alternating magnet array with tunable gap which is potentially simple and cheap.

5.   Conclusion

We introduced a new method for controlling the longitudinal phase space using phase space exchange. The capability and quality control of the temporal profile shaping is successfully demonstrated by the single EEX beamline at AWA. This work was recently extended to demonstrate high transformer ratio which is one of the most important issues for the wakefield accelerator community. The AWA facility plans to explore other possible applications of exchange based manipulation in near future. A double EEX beamline is under construction and will be used to demonstrate shaping, bunch compression, frequency up/down shift, and train generation. The four applications introduced here potentially provide additional benefits over existing methods.

The emittance exchange beamline is a powerful tool for controlling the longitudinal phase space with the relatively easier methods of transverse phase space control. Exchange based manipulation potentially overcomes the quality and capability limitations of laser-based and coupling-based methods. We hope this method overcomes some of the limits of present accelerators to open up new undiscovered areas.

Acknowledgments

References

1.   K. Bane, P. Chen, and P. B. Wilson, On collinear wakefield acceleration, IEEE Trans. Nucl. Sci. 32, 3524 (1985).

2. A. Zholents et al., A collinear wakefield accelerator for a high repetition rate multi beamline soft X-ray FEL facility, in Proceedings of FEL2014, Basel, Switzerland 2014 (JACoW, Geneva, 2014).

3. A. Zholents et al., A preliminary design of the collinear dielectric wakefield accelerator, Nucl. Instrum. Methods Phys. Res., Sect. A 829, 190 (2016).

4. M. Dunning et al., Generating periodic terahertz structures in a relativistic electron bunch through frequency down-conversion of optical lasers, Phys. Rev. Lett. 109, 074801 (2012).

5. Y.-E Sun et al., Tunable subpicosecond electron-bunch-train generation using a transverse-to-longitudinal phase-space exchange technique, Phys. Rev. Lett. 105, 234801 (2010).

6. J. G. Power and C. Jing, Temporal laser pulse shaping for RF photocathode guns: the cheap and easy way using UV birefringent crystals, AIP Conf. Proceedings 1086, 689 (2009).

7. P. Muggli, V. Yakimenko, M. Babzien, E. Kallos, and K. P. Kusche, Generation of trains of electron microbunches with adjustable subpicosecond spacing, Phys. Rev. Lett. 101, 054801 (2008).

8. G. Andonian et al., Generation of ramped current profiles in relativistic electron bunchs using wakefields in dielectric structures, Phys. Rev. Lett. 118, 054802 (2017).

9. S. Antipov et al., Subpicosecond bunch train production for a tunable mJ level THz source, Phys. Rev. Lett. 111, 134802 (2013).

10. P. Emma, Z. Huang, K.-J. Kim and P. Piot, Transverse-to-longitudinal emittance exchange to improve performance of high-gain free-electron lasers, Phys. Rev. ST Accel. Bunchs 9, 100702 (2006).

11. P. Piot, Y.-E Sun, J. G. Power, and M. Rihaoui, Generation of relativistic electron bunches with arbitrary current distribution via transverse-to-longitudinal phase space exchange, Phys. Rev. ST Accel. Bunchs 14, 022801 (2011).

12. G. Ha, M. H. Cho, W. Gai, K.-J. Kim , W. Namkung and J. G. Power, Perturbation-minimized triangular bunch for high-transformer ratio using a double dogleg emittance exchange bunch line, Phys. Rev. Accel. Bunchs 19, 121301 (2016).

13. G. Ha, J. G. Power, M. Conde, D. S. Doran, and W. Gai, Preparations for installation of the double emittance-exchange beamline at the Argonne Wakefield Accelerator facility, in Proceedings of FEL2017, Santa Fe, NM 2017 (JACoW, Geneva, 2017).

14. G. Ha, J. G. Power, M. Conde, D. S. Doran, and W. Gai, Limiting effects in double EEX beamline, Journal of Physics: Conf. Series 874, 012061 (2017).

15. G. Ha et al., Precision control of the electron longitudinal bunch shape using an emittance-exchange bunch line, Phys. Rev. Lett. 118, 104801 (2017).

16. G. Ha, J. G. Power, M. Conde, D. S. Doran, and W. Gai, Simultaneous generation of drive and witness bunch for collinear wakefield acceleration, Journal of Physics: Conf. Series 874, 012027 (2017).

17. G. Ha, J. G. Power, M. Conde, D. S. Doran, and W. Gai, Preliminary simulations on chirp-less bunch compression using double-EEX beamline, in Proceedings of IPAC2017, Copenhagen, Denmark 2017 (JACoW, Geneva, 2017).
18. Q. Gao et al., under review process.
19. M. Cornacchia and P. Emma, Transverse to longitudinal emittance exchange, Phys. Rev. ST Accel. Bunchs 5, 084001 (2002).
20. D. Y. Shchegolkov and E. I. Simakov, Design of an emittance exchanger for production of special shapes of the electron bunch current, Phys. Rev. ST Accel. Bunchs 17, 041301 (2014).
21. A. Zholents and M. S. Zolotorev, A new type of bunch compressor and seeding of a short wave length coherent radiation, Report No. ANL-APS-LS-327, 2011.
22. R. Kato et al., Suppression and enhancement of coherent synchrotron radiation in the presence of two parallel conducting plates, Phys. Rev. E 57, 3454 (1988).
23. I. V. Bazarov and T. Miyajima, Calculation of coherent synchrotron radiation in general particle tracer, in Proceedings of EPAC2008, Genoa, Italy 2008.
24. M. Conde et al., Research program and recent results at the Argonne Wakefield Accelreator facility (AWA), in Proceedings of IPAC2017, Copenhagen, Denmark 2017 (JACoW, Geneva, 2017).
25. B. Jiang, C. Jing, P. Schoessow, J. Power, and W. Gai, Formation of a novel shaped bunch to enhance transformer ratio in collinear wakefield accelerators, Phys. Rev. ST Accel. Beams 15, 011301 (2012).
26. F. Lemery and P. Piot, Tailored electron bunches with smooth current profiles for enhanced transformer ratio in beam-driven acceleration, Phys. Rev. ST Accel. Beams 18, 081301 (2015).
27. P. Piot et al., Generation and characterization of electron bunches with ramped current profiles in a dual-frequency superconducting linear accelerator, Phys. Rev. Lett. 108, 034801 (2012).
28. Q. Gao et al., in preparation.
29. Linac Coherent Light Source (LCLS) conceptual design report.
30. G. Ha, Longitudinal density profile shaping using double dog-leg emittance exchange beamline, PhD thesis, POSTECH (2017).